Contribution from the Department of Chemistry,
Texas A&M University, College Station, Texas 77843

Electronic Structure of Metal Clusters. 5. Photoelectron Spectra and Molecular Orbital Calculations of Hydrogen- and Halogen-Bridged Triosmium Decacarbonyls

PETER T. CHESKY and MICHAEL B. HALL*

Received February 15, 1983

The gas-phase, ultraviolet photoelectron (PE) spectra and molecular orbital (MO) calculations are reported for (μ-H)(μ-X)$Os_3(CO)_{10}$ and (μ-X)$_2Os_3(CO)_{10}$ (X = Cl, Br, I). We observe a loss of intensity in the ionization region of the Os–Os bonds compared to that of $Os_3(CO)_{12}$. The MO calculations suggest that the only direct Os–Os bonds in both of these bridging series are the two $(CO)_4Os$–$Os(CO)_3$ bonds. The $(CO)_3Os$–$Os(CO)_3$ interaction in the (μ-H)(μ-X) series is weakly bonding, while that in the (μ-X)$_2$ series is weakly antibonding. Shifts in the positions of the ionizations due to the t_{2g}-like orbitals are observed. The MO calculations suggest that the t_{2g}-like $Os(CO)_3$ orbitals, which are usually considered only M–CO π bonding, interact strongly with the bridging H and halogen atoms to produce the observed shifts.

Introduction

There has been considerable interest in the structure of (μ-H)(μ-X)$Os_3(CO)_{10}$ (X = H, Cl, Br, OMe, NO), (μ-X)$_2Os_3(CO)_{10}$ (X = H, Br, OMe), and related compounds.[1] Churchill et al. have shown that metal–metal bonds, bridged by both H and another ligand, may result in the metal–metal distance being longer or shorter than the nonbridged metal–metal distances within the same compound.[2] Recently, it has been shown that the presence of H ligands in higher nuclearity osmium clusters produces unusual metal geometries,[3] which cannot be rationalized by skeletal electron-counting procedures.[4] Mason and Mingos presented a qualitative symmetry-based treatment on (μ-H)$_2$-, (μ-OMe)(μ-H)-, and (μ-OMe)$_2Os_3(CO)_{10}$ complexes to explain the interaction between the bridging ligands and the metal d orbitals.[5] They suggested that the (μ-H)$_2$ cluster is electron deficient and requires a multiple metal–metal bond between the bridging osmium atoms to obey the 18-electron rule. The (μ-H)(μ-OMe) cluster requires only a single metal–metal bond between the bridging osmium atoms, while the (μ-OMe)$_2$ cluster is electron rich and does not require a metal–metal bond. Approximate molecular orbital calculations have been performed on both dinuclear and trinuclear transition-metal species to provide an explanation for the effect of bridging ligands on metal–metal bonds.[6]

Clusters with the formulas (μ-H)(μ-X)$Os_3(CO)_{10}$ and (μ-X)$_2Os_3(CO)_{10}$ (X = Cl, Br, I) represent two common classes of triosmium compounds.[7] The (μ-X)$_2Os_3(CO)_{10}$ clusters have been prepared from heating $Os_2(CO)_8X_2$ (X = Cl, Br) under vacuum,[8] reacting 2-(bromoethyl)naphthalene with $Os_3(CO)_{12}$,[1j] thermolysis of (μ-X)$_2Os_3(CO)_{12}$ (X = Cl, Br),[8,9] and reacting allylic halides with (μ-H)$_2Os_3(CO)_{10}$.[10] The (μ-H)(μ-X)$Os_3(CO)_{10}$ clusters have been prepared by reacting HX with $Os_3(CO)_{12}$,[11] $(NCCH_3)_2Os_3(CO)_{10}$,[12] and $(C_6H_8)Os_3(CO)_{10}$.[13] The HX species react with $Os_3(CO)_{12}$ in the presence of an amine oxide, forming (H)(X)$Os_3(CO)_{11}$, which readily forms (μ-H)(μ-X)$Os_3(CO)_{10}$.[14] During catalytic carbon monoxide hydrogenation over $Os_3(CO)_{12}$ and BBr_3, it was established that (μ-Br)$_2Os_3(CO)_{10}$ was formed.[15]

The structure of (μ-H)(μ-Cl)$Os_3(CO)_{10}$ (**1**) was first proposed from the results obtained from IR and mass spectroscopy.[9] The mass spectroscopic measurements verified the presence of H by the m/e of the parent peak. The absence of a (mass − Cl)$^+$ fragment peak suggested a bridging Cl ligand. The X-ray structure confirmed the triangular arrangement of Os carbonyl fragments with two bridging ligands, H and Cl. The presence of the bridging Cl was shown to counterbalance the bridging H ligand's effect on the metal–metal bond distance.[1f] The Os–Os distances in (μ-H)$_2Os_3(CO)_{10}$ are 2.683 and 2.815 Å,[1e] while the Os–Os distances in (μ-H)(μ-Cl)$Os_3(CO)_{10}$[1f] are 2.846 and 2.832 Å for the bridged and nonbridged, respectively. When a second halogen replaces the H, as in (μ-Cl)$_2Os_3(CO)_{10}$, the Os–Os distances are 3.233 and 2.852 Å for the bridged and nonbridged bonds, respectively.[1k]

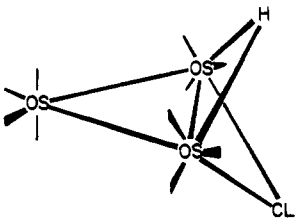

1

Although several review articles have appeared that summarize the preparation and structure of (μ-H)(μ-X)$Os_3(CO)_{10}$ and (μ-X)$_2Os_3(CO)_{10}$ (X = Cl, Br, I) clusters,[7,16] only a few

(1) (a) Johnson, B. F. G.; Lewis, J.; Kilty, P. A. *J. Chem. Soc.* **1963**, 2859. (b) Allen, V. F.; Mason, R.; Hitchcock, P. B. *J. Organomet. Chem.* **1977**, *140*, 297. (c) Churchill, M. R.; Hollander, F. J.; Hitchison, T. P. *Inorg. Chem.* **1977**, *16*, 2260. (d) Orpen, G.; Rivera, A. V.; Bryan, E. G.; Pippard, D.; Sheldrick, G. M. J. *J. Chem. Soc., Chem. Commun.* **1978**, 723. (e) Broach, R. W.; Williams, J. W. *Inorg. Chem.* **1979**, *18*, 314. (f) Churchill, M. R.; Lashewycz, R. A. *Ibid.* **1979**, *18*, 1926. (g) Churchill, M. R.; Lashewycz, R. A. *Ibid.* **1979**, *18*, 3261. (h) Johnson, B. F. G.; Raithby, P. R.; Zuccaro, C. *J. Chem. Soc., Dalton Trans.* **1980**, 99. (i) Churchill, M. R.; Wasserman, H. J. *Inorg. Chem.* **1980**, *19*, 2391. (j) Aleksandrov, G. G.; Zol'nikova, G. P.; Kritskaya, I. I.; Struchkow, Y. T. *Koord. Khim.* **1980**, *6*, 626. (k) Einstein, F. W. B.; Jones, T.; Tyers, K. G. *Acta Crysta..ogr., Sect. B* **1982**, *B38*, 1272.

(2) Churchill, M. R.; DeBoer, B. G.; Rotella, F. J. *Inorg. Chem.* **1976**, *15*, 1843.

(3) Braga, D.; Henrick, K.; Johnson, B. F. G.; Lewis, J.; McPartlin, M.; Nelson, W. J. H.; Vargas, M. D. *J. Chem. Soc., Chem. Commun.* **1982**, 419.

(4) (a) Mason, R.; Thomas, K. M.; Mingos, D. M. P. *J. Am. Chem. Soc.* **1973**, *95*, 3802. (b) Eady, C. R.; Johnson, B. F. G.; Lewis, J. *J. Chem. Soc., Dalton Trans.* **1975**, 2606. (c) Lauher, J. W. *J. Am. Chem. Soc.* **1978**, *100*, 5305. (d) Lauher, J. W. *Ibid.* **1979**, *101*, 2604.

(5) Mason, R.; Mingos, D. M. P. *J. Organomet. Chem.* **1973**, *50*, 53.

(6) (a) Teo, B. K.; Hall, M. B.; Fenske, R. F.; Dahl, L. F. *J. Organomet. Chem.* **1974**, *70*, 413. (b) Pinhas, A. R.; Albright, T. A.; Hoffmann, R. *Helv. Chim. Acta* **1980**, *63*, 29. (c) Hoffman, D. M.; Hoffmann, R. *Inorg. Chem.* **1981**, *20*, 3543.

(7) Seddon, E. R. *Coord. Chem. Rev.* **1982**, *41*, 159.

(8) Demming, A. J.; Johnson, B. F. G.; Lewis, J. *J. Chem. Soc. A* **1970**, 897.

(9) Demming, A. J.; Johnson, B. F. G.; Lewis, J. *J. Organomet. Chem.* **1969**, *17*, P40.

(10) Demming, A. J.; Hasso, S. *J. Organomet. Chem.* **176**, *114*, 313.

(11) Azam, K. A.; Demming, A. J.; Kimber, R. E.; Sukla, P. R. *J. Chem. Soc., Dalton Trans.* **1976**, 1853.

(12) Tachikawa, M.; Shapley, J. R. *J. Organomet. Chem.* **1977**, *124*, C19.

(13) Bryan, E. G.; Johnson, B. F. G.; Lewis, J. *J. Chem. Soc., Dalton Trans.* **1977**, 1328.

(14) Johnson, B. F. G.; Lewis, J.; Pippard, D. *J. Organomet. Chem.* **1978**, *145*, C4.

(15) Choi, H. W.; Muetterties, E. L. *Inorg. Chem.* **1981**, *20*, 2664.

0020-1669/83/1322-3327$01.50/0

other chemical measurements have appeared for these triosmium decacarbonyl compounds. Variable-temperature ^{13}C NMR on $(\mu\text{-X})_2Os_3(CO)_{10}$ (X = Cl, Br, I) indicated that CO exchanges between the bridged Os atoms, but not between the bridged Os atoms and the Os atom in the $Os(CO)_4$ fragment.[17] The results of a similar study on $(\mu\text{-H})(\mu\text{-X})Os_3(CO)_{10}$ (X = Cl, Br, I) hinted that no exchange of CO's occurs between either of the two bridged Os atoms.[18] Negative-ion mass spectroscopy verified that $(\mu\text{-X})_2Os_3(CO)_{12}$ readily loses CO to form the more stable $(\mu\text{-X})_2Os_3(CO)_{10}$ cluster.[19]

Further interest in the triosmium decacarbonyl clusters comes from the proposed correspondence between discrete metal clusters as models for transition-metal surfaces or highly dispersed, supported catalysts.[20,21] Recently, triosmium decacarbonyl clusters have been successfully anchored to high-surface-area oxides.[22]

This study will investigate the bonding in $(\mu\text{-H})(\mu\text{-X})Os_3(CO)_{10}$ and $(\mu\text{-X})_2Os_3(CO)_{10}$ (X = Cl, Br, I) series using gas-phase, ultraviolet photoelectron (PE) spectroscopy. This technique has been useful in determining the electronic structures of transition-metal compounds.[23,24] The PE spectral will be interpreted by observing the trends in derivatives within the same series and by comparing these trends with the results from parameter-free Fenske–Hall molecular orbital (MO) calculations.[25] By employing the MO calculations and the PE spectra, we will develop a consistent picture of the electronic structures and bonding within these two triosmium decacarbonyl series. The $(X)_2Os_3(CO)_{12}$ (X = Cl, Br, I) clusters were also attempted, but they readily decomposed in the spectrometer.

Experimental and Theoretical Section

Preparation. The $(\mu\text{-H})(\mu\text{-X})Os_3(CO)_{10}$ and $(\mu\text{-X})_2Os_3(CO)_{10}$ (X = Cl, Br, I) compounds were generously provided by Professor Jack Lewis.

Spectroscopy. The gas-phase, ultraviolet photoelectron spectra were taken on a Perkin-Elmer Model PS-18 spectrometer. The spectra were recorded as a single slow scan, and the argon $^2P_{3/2}$ and $^2P_{1/2}$ lines at 15.76 and 15.94 eV were used as an internal reference. The resolution for all spectra was better than 35 meV for the fwhm of the Ar $^2P_{3/2}$ peak. The free CO spike at 14 eV was not observed, indicating that all compounds were stable and did not decompose in the spectrometer.

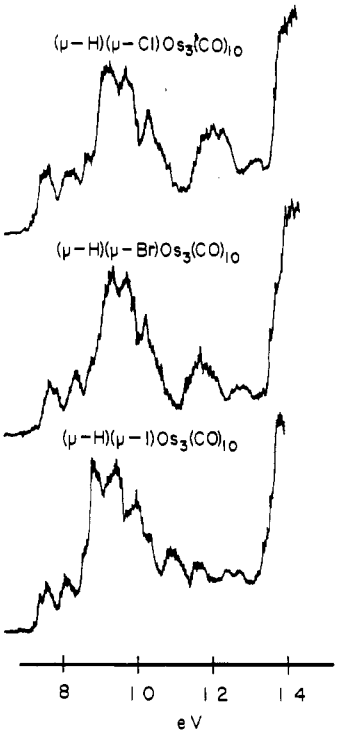

Figure 1. Partial photoelectron spectra of $(\mu\text{-H})(\mu\text{-X})Os_3(CO)_{10}$ (X = Cl, Br, I).

Table I. Absolute Values for PE Ionization Peak Maxima (eV) in $(\mu\text{-H})(\mu\text{-X})Os_3(CO)_{10}$ (X = Cl, Br, I)[a]

bands	chloro	bromo	iodo
1	7.6 (w)	7.6 (w)	7.5 (w)
	8.2 (w)	8.3 (w)	8.1 (w)
	8.6 (w)	8.6 (w)	8.6 (w)
2	9.2 (s)	9.3 (s)	8.8 (s)
	9.7 (s)	9.7 (s)	9.4 (s)
	10.4	10.3	10.1
3	12.1	11.7	10.9
	12.3	12.1	11.6
	12.8–13.2 (w)	12.5–13.0 (w)	12.2–12.8 (w)

[a] w = weak intensity; s = strong intensity.

Theoretical Procedures. Fenske–Hall MO calculations[25] (nonempirical, self-consistent field) were performed on an Amdahl 470 V/6 computer at Texas A&M University. Since there are no suitable Os functions available, the actual calculations were performed on the Ru analogues, but we will refer to the results as if they were on the Os clusters. The ruthenium basis functions ($4d^7$) were taken from Richardson et al.[26] and were augmented by 5s and 5p functions with exponents of 2.20. The carbon, oxygen, and halogen functions were taken from the double-ζ functions of Clementi[27] and reduced to a single-ζ function,[28] except for the p valence functions, which were retained as the double-ζ function. An exponent of 1.2 was used for the hydrogen atom. The atomic functions were made orthogonal by the Schmidt procedure. Mulliken population analysis was used to determine both the individual atomic charges and the atomic orbital populations.

The atomic positions for $(\mu\text{-H})(\mu\text{-X})Os_3(CO)_{10}$ (X = Cl, Br, I) were taken from the crystal structures by Churchill et al.[1f,g] and were idealized to C_s symmetry. The hydrogen atoms were placed such that the Os–H distances were 1.92 Å. This value is the average between the distance determined by a difference-Fourier map during the solution of the bromo derivative's crystal structure (2.03 Å)[1g] and that from the neutron diffraction studies of $(\mu\text{-H})_2Os_3(CO)_{10}$ (1.845

(16) (a) Lewis, J.; Johnson, B. F. G. *Pure Appl. Chem.* **1975**, *44*, 43. (b) Johnson, B. F. G. *Platinum Met. Rev.* **1978**, *22*, 47. (c) Lewis, J.; Johnson, B. F. G. *Gazz. Chim. Ital.* **1979**, *109*, 271.
(17) Bryan, E. G.; Johnson, B. F. G. Lewis, J. *J. Chem. Soc., Chem. Commun.* **1977**, 329.
(18) Bryan, E. G.; Forster, A.; Johnson, B. F. G.; Lewis, J.; Matheson, T. W. *J. Chem. Soc., Dalton Trans.* **1978**, *196*.
(19) Vaglio, G. A. *J. Organomet. Chem.* **1979**, *169*, 83.
(20) Woolley, R. G. *Platinum Met. Rev.* **1980**, *24*, 26.
(21) (a) Tolman, C. A. *Chem. Soc. Rev.* **1972**, *1*, 337. (b) Ugo, R. *Catal. Rev.—Sci. Eng.* **1975**, *11*, 225. (c) Muetterties, E. L. *Bull. Soc. Chim. Belg.* **1975**, *84*, 959. (d) Muetterties, E. L. *Ibid.* **1976**, *85*, 451. (e) Muetterties, E. L.; Rhodin, T. N.; Band, E.; Brucker, C. F.; Pretzer, W. R. *Chem. Rev.* **1979**, *79*, 91. (f) Chini, P. *Gazz. Chim. Ital.* **1979**, *109*, 225. (g) Ertl, G. *Ibid.* **1979**, *109*, 217. (h) Muetterties, E. L. *Isr. J. Chem.* **1980**, *20*, 84. (i) Evans, J. *Chem. Soc. Rev.* **1981**, *10*, 159. (j) Muetterties, E. L. *Catal. Rev.—Sci. Eng.* **1981**, *23*, 69. (k) Muetterties, E. L. *Inorg. Chim. Acta* **1981**, *50*, 1.
(22) (a) Evans, J.; Gracey, B. P. *J. Chem. Soc., Chem. Commun.* **1980**, 852. (b) Castrillo, T.; Knozinger, H.; Wolf, M. *Inorg. Chim. Acta* **1980**, *45*, L235. (c) Evans, J.; Gracey, B. P. *J. Chem. Soc., Dalton Trans.* **1982**, 1123.
(23) (a) Turner, D. W.; Baker, C.; Baker, A. D.; Brundle, C. R. "Molecular Photoelectron Spectroscopy", 1st ed.; Wiley: New York, 1970. (b) Rabalais, J. W. "Principles of Ultraviolet Photoelectron Spectroscopy", 1st ed.; Wiley: New York, 1977. (c) Cowley, A. H. *Prog. Inorg. Chem.* **1980**, *26*, 45.
(24) (a) Chesky, P. T.; Hall, M. B. *Inorg. Chem.* **1981**, *20*, 4419 (part one). (b) Sherwood, D. E., Jr.; Hall, M. B. *Ibid.* **1982**, *21*, 3458 (part two). (c) Sherwood, D. E., Jr.; Hall, M. B. *Organometallics* **1982**, *1*, 1519 (part three).
(25) Hall, M. B.; Fenske, R. F. *Inorg. Chem.* **1972**, *11*, 768.
(26) Richardson, J. W.; Blackman, M. J.; Ranochak, J. E. *J. Chem. Phys.* **1973**, *58*, 3010.
(27) (a) Clementi, E. J. *J. Chem. Phys.* **1964**, *40*, 1944. (b) Clementi, E. J. *IBM J. Res. Dev.* **1965**, *9*, 2.
(28) Fenske, R. F.; Radtke, D. D. *Inorg. Chem.* **1968**, *7*, 479.

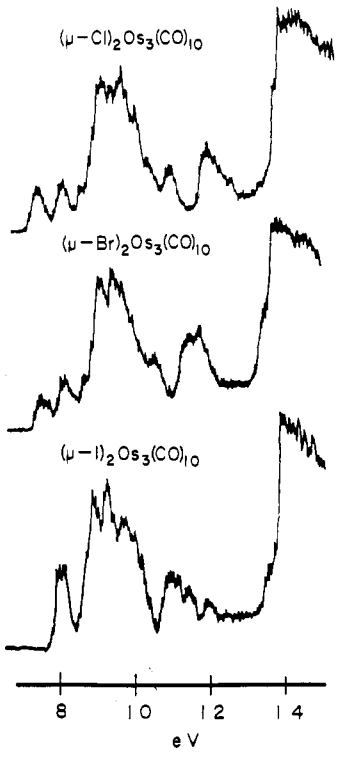

Figure 2. Partial photoelectron spectra of $(\mu\text{-X})_2Os_3(CO)_{10}$ (X = Cl, Br, I).

Å).[1e] The atomic positions for $(\mu\text{-X})_2Os_3(CO)_{10}$ (X = Cl, Br, I) were determined from the crystal structures of the bromo and chloro derivatives and were idealized to C_{2v} symmetry.[1j,k] Since Ru–X and Os–X distances are nearly the same, these Os distances were used in the calculation, which are actually on Ru clusters.

Results

Photoelectron Spectra. The ionization energy (IE) range of interest spans 7–14 eV. The IE region above 14 eV will not be discussed because of the normally broad and poorly resolved bands due to the carbonyls' 5σ and 1π ionizations.

The partial photoelectron spectra of $(\mu\text{-H})(\mu\text{-X})Os_3(CO)_{10}$ (X = Cl, Br, I) are shown in Figure 1. These spectra are characterized by a series of weak ionization peaks occurring before the strong ionization, which is split into a doublet. A broad shoulder occurring on the high-energy side of this doublet contains a sharp ionization peak. A small energy gap separates the shoulder from the next ionization band(s). A weaker ionization band occurs between 12 and 13.2 eV. A small energy gap separates these weak bands from the intense region corresponding to CO ionization. The location of the IE peaks for these clusters are summarized in Table I.

The partial spectra of $(\mu\text{-X})_2Os_3(CO)_{10}$ (X = Cl, Br, I) are shown in Figure 2. These spectra are characterized by small ionization peak(s) occurring before an intense wide manifold consisting of many closely spaced peaks. A small energy gap separates the shoulder on the high-energy side of the ionization manifold from a moderately intense ionization band. A larger energy gap separates this ionization band from the free CO region. The locations of the IE peaks for these clusters are listed in Table II.

Molecular Orbital Calculations. In large molecules such as triosmium decacarbonyl clusters, the complexity of the MO pattern becomes difficult to interpret because of the large number of closely spaced MO's. One can simplify this problem by analyzing the molecule's MO's in terms of smaller components. One approach is fragment analysis, where one views the triosmium decacarbonyl clusters as formed from two $Os(CO)_3$ units, one $Os(CO)_4$, and the diatomic molecule that consists of the two bridging atoms. This approach has been successfully applied to describe the bonding in trimetallic nonacarbonyl clusters.[24] The numbering of the molecular orbitals of the clusters and fragments begins with the lowest energy valence molecular orbitals, except for the carbonyls and bridging diatomic species where the numbering begins with the first core level.

The metal orbitals of the $Os(CO)_3$ and $Os(CO)_4$ fragments can be classified as t_{2g}- or e_g-like.[29] The t_{2g}-like set, which has d orbitals with lobes between the Os–C internuclear axis, is stabilized by Os d_π to CO 2π back-donation. The e_g-like set, which has d orbitals with lobes along the Os–C internuclear axis, is destabilized by CO 5σ to Os d_σ donation. The t_{2g}–e_g splitting ($10Dq$) is large, which is consistent with the large crystal field splitting expected for the CO ligand and a second- or third-row transition metal.[30]

Table II. Absolute Values for PE Ionization Peak Maxima (eV) in $(\mu\text{-X})_2Os_3(CO)_{10}$ (X = Cl, Br, I)[a]

bands	chloro	bromo	iodo
1	7.3 (w)	7.4 (w)	
	8.0 (w)	8.0 (w)	8.0 (s)
2	8.6 (w)	8.6 (w)	
	9.0 (s)	8.9 (s)	8.8 (s)
	9.6 (s)	9.5 (s)	9.4 (s)
	9.9 (s)	9.8 (s)	9.7 (s)
	10.1		
	10.8 (w)	10.6 (w)	10.2
3	11.9	11.4	10.9
	12.4	11.7	11.1
			11.4 (w)
			11.9 (w)

[a] w = weak intensity; s = strong intensity.

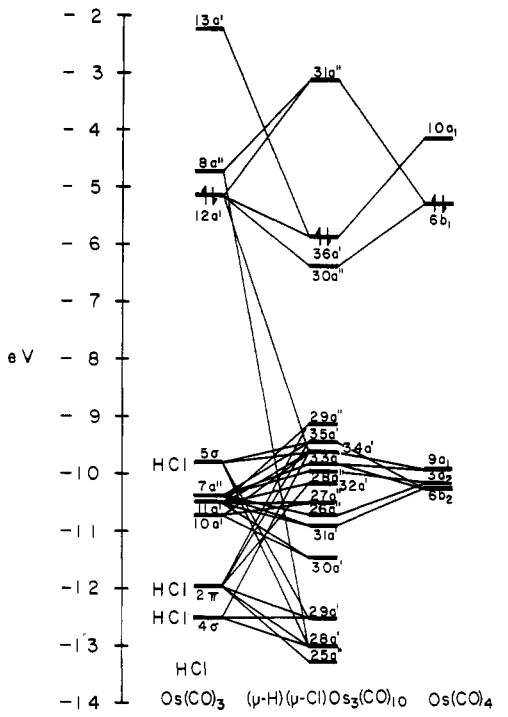

Figure 3. Molecular orbital bonding scheme for $(\mu\text{-H})(\mu\text{-Cl})Os_3(CO)_{10}$. The energy values were obtained from a Fenske–Hall calculation. Connectivity lines indicate the principal contributions to each molecular orbital.

(29) (a) Elian, M.; Hoffmann, R. *Inorg. Chem.* **1975**, *14*, 1058. (b) Hoffmann, R. *Science (Washington, D.C.)* **1981**, *211*, 995 and references within. (c) Hoffmann, R. *Angew. Chem., Int. Ed. Engl.* **1982**, *21*, 711.

(30) (a) Ballhausen, C. J. "Introduction to Ligand Field Theory", 1st ed.; McGraw-Hill: New York, 1962. (b) Figgis, B. N. "Introduction to Ligand Fields", 1st ed.; Wiley-Interscience: New York, 1966. (c) Cotton, F. A.; Wilkinson, G. "Advanced Inorganic Chemistry", 4th ed.; Wiley-Interscience: New York, 1980.

Table III. Atomic Composition of the $Os(CO)_3$ Fragment

	% atomic compn				
orbital	d	s	p	CO 5σ	CO 2π
13a′	11	21	31		33
8a″ (LUMO)	43		33	6	18
12a′ (HOMO)	44		31	4	17
7a″	75				21
11a′	74				22
10a′	73				24

Table IV. Atomic Composition of the $Os(CO)_4$ Fragment

	% atomic compn				
orbital	d	s	p	CO 5σ	CO 2π
$10a_1$ (LUMO)	19	11	28	2	40
$6b_1$ (HOMO)	38		27	5	30
$9a_1$	77				22
$3a_2$	72				26
$6b_2$	71				27

$(\mu$-H)$(\mu$-X)$Os_3(CO)_{10}$ (X = Cl, Br, I). Although MO calculations were made on all of the compounds, only the electronic structure of (μ-chloro)(μ-hydrido)decacarbonyltriosmium (Figure 3) will be discussed in detail. The other compounds in this series are closely related, and only the more important, less obvious differences will be noted. The $Os(CO)_3$ and $Os(CO)_4$ fragments were idealized to C_s and C_{2v}, respectively. The lowest lying molecular orbitals of the Os carbonyl fragments consist of symmetry-adapted combinations of the carbonyls' 3σ, 4σ, and 1π and the Os–CO σ bonds formed by donation from the carbonyls' 5σ to metal orbitals.

In $Os(CO)_3$ the next group of orbitals (10a′, 11a′, 7a″) occur at much higher energy than the Os–CO σ orbitals and are predominantly Os d. These orbitals, which are stabilized by the carbonyls' 2π, correspond to the t_{2g}-like orbitals of an octahedral (O_h) system. The next two orbitals (12a′, 8a″) correspond to the e_g-like orbitals of an O_h system. These two orbitals are destabilized by some carbonyl 5σ donation. We will assume that in the neutral $Os(CO)_3$ fragment 12a′ (HOMO) is doubly occupied. If 8a″ and 12a′ were degenerate and each singly occupied, 13a′ would be the LUMO. The 8a″ and 13a′ orbitals contain more Os diffuse s and p than compact d character. The most important fragment orbitals for the formation of the cluster have their atomic characters listed in Table III.

The $Os(CO)_4$ fragment's t_{2g}-like orbitals ($6b_2$, $3a_2$, $9a_1$) are higher in energy than the Os–CO σ orbitals. The t_{2g}-like orbitals are predominantly Os d and are stabilized by the carbonyls' 2π. Occurring at higher orbital energies are $6b_1$ and $10a_1$, which correspond to the O_h e_g-like orbitals. These two orbitals are destablized by the CO 5σ. We will assume that in the neutral fragment $6b_1$ is the doubly occupied HOMO, while $10a_1$ is the LUMO. The most important fragment orbitals for the formation of the cluster have their atomic character listed in Table IV.

The two bridging atoms may be thought of as an elongated diatomic molecule. The HCl molecule's 4σ consists of Cl $3p_z$ (64%), Cl 3s (13%), and H (23%). The doubly occupied HOMO, 2π, is composed of Cl $3p_x$ and $3p_y$. The LUMO, 5σ, contains Cl $3p_z$ (49%) and H (51%).

The $(\mu$-H)$(\mu$-Cl)$Os_3(CO)_{10}$ cluster formation will be described in terms of the higher energy orbitals of the two $Os(CO)_3$, the $Os(CO)_4$, and the HCl fragments' molecular orbitals. Despite the fact that lower energy fragment orbitals may be delocalized over the entire cluster, they do not contribute to the cluster formation. The MO diagram for the formation of $(\mu$-H)$(\mu$-Cl)$Os_3(CO)_{10}$ from the fragments is shown in Figure 3.

The HOMO in $(\mu$-H)$(\mu$-Cl)$Os_3(CO)_{10}$, 36a′, and the orbital directly under it, 30a″, represent the two unbridged Os–Os bonds. These orbitals are composed primarily of the fragments' e_g-like orbitals. An energy gap separates these two orbitals from a broad manifold of closely spaced molecular orbitals. This manifold is composed of the group of orbitals that represent Os t_{2g}-like interactions and some destabilized HCl character. Another small energy gap separates this broad manifold from the lower three molecular orbitals, which represent Os–Cl–Os mixed with some Os–H–Os interactions. The compositions of the $(\mu$-H)$(\mu$-Cl)$Os_3(CO)_{10}$ molecular orbitals are listed in Table V.

The formation of the cluster will be presented in terms of the t_{2g}- and e_g-like fragment orbitals. In the neutral $Os(CO)_3$ and $Os(CO)_4$ fragments, the orbital populations are $(10a')^{2.0}(11a')^{2.0}(7a'')^{2.0}(12a')^{2.0}(8a'')^{0.0}(13a')^{0.0}$ and $(6b_2)^{2.0}$-$(3a_2)^{2.0}(9a_1)^{2.0}(6b_1)^{2.0}(10a_1)^{0.0}$, respectively. The final cluster populations for $Os(CO)_3$ and $Os(CO)_4$ are $(10a')^{2.0}(11a')^{2.0}$-$(7a'')^{2.0}(12a')^{0.9}(8a'')^{0.4}(13a')^{0.3}$ and $(6b_2)^{2.0}(3a_2)^{2.0}(9a_1)^{2.0}$-$(6b_1)^{1.1}(10a_1)^{0.9}$, respectively. Accounting for the net loss of electron population in the two $Os(CO)_3$ fragments, the HCl 5σ gains electron density. The elongated HCl has a population of $(4\sigma)^{2.0}(2\pi)^{4.0}(5\sigma)^{0.0}$ before cluster formations and a population of $(4\sigma)^{1.6}(2\pi)^{3.6}(5\sigma)^{1.5}$ after cluster formation. The increased population of 5σ breaks the H–Cl bond.

$(\mu$-X)$_2Os_3(CO)_{10}$ (X = Cl, Br, I). Only the electronic structure of bis(μ-chloro)decacarbonyltriosmium (Figure 4) will be presented in detail. The $Os(CO)_3$ and $Os(CO)_4$ fragments are identical with those described above. The elongated, bridging diatomic Cl_2 molecule's $5\sigma_g$ orbital is pure

Table V. Molecular Composition of $(\mu$-H)$(\mu$-Cl)$Os_3(CO)_{10}$

	% fragment compn													
	$Os(CO)_3$						$Os(CO)_4$					HCl		
orbital	13a′	8a″	12a′	7a″	11a′	10a′	$10a_1$	$6b_1$	$9a_1$	$3a_2$	$6b_2$	5σ	2π	4σ
31a″ (LUMO)	2	37	30					27					2	
36a′ (HOMO)	16		33				46							4
30a″		2	38					55					1	
29a″		7		8	55	12							13	
35a′	2	5	3	28		6		13	4			18	11	8
34a′		8	8	4	19	10			17			11	4	17
33a′				12	2	2			60		13	2	1	5
28a″				30	5	2				61				
32a′					14	5			12		52	4	10	
27a″					17	81								
26a″				60	3					37				
31a′				45	25	5		21				2		
30a′	3				28	61			5			1		
29a′			3	7	7	6						13	23	37
28a′	3	8	2	2		4						22	31	22
25a″	2	6	2	2	16								69	

Table VI. Molecular Composition of $(\mu\text{-Cl})_2Os_3(CO)_{10}$

	% fragment compn													
	$Os(CO)_3$						$Os(CO)_4$					Cl_2		
orbital	13a′	8a″	12a′	7a″	11a′	10a′	$10a_1$	$6b_1$	$9a_1$	$3a_2$	$6b_2$	$5\sigma_u$	$2\pi_g$	$2\pi_u$	$5\sigma_g$
$19b_1$ (LUMO)	8		48					23						6	
$24a_1$ (HOMO)	10		41				43								2
$18b_1$	11		31					54						1	
$23a_1$					2	29			62					4	1
$16b_2$				44							52			3	1
$11a_2$				34						64			1		
$17b_1$			5		66	17								10	
$22a_1$			1		53	5			21					16	4
$15b_2$				31							42	2	24		
$16b_1$					20	80									
$10a_2$				62						36			1		
$21a_1$				29	43				14					8	3
$14b_2$		4		14							2	58	18		
$20a_1$					7	21			2					63	2
$13b_2$		11		9							4	23	48		
$9a_2$		17		4								76			
$15b_1$		5	6		13	3								71	
$19a_1$	6		5		6	1								2	78

Cl $3p_z$. At slightly higher orbital energies are the $2\pi_u$ and $2\pi_g$ (HOMO) orbitals. The $2\pi_u$ and $2\pi_g$ orbitals are pure Cl 3p bonding and antibonding, respectively. The LUMO, $5\sigma_u$, is pure Cl $3p_z$ in character.

The $(\mu\text{-Cl})_2Os_3(CO)_{10}$ cluster formation will be presented in terms of the higher orbitals of the two $Os(CO)_3$, the $Os(CO)_4$, and the Cl_2 fragments' molecular orbitals. The O_h t_{2g}- and e_g-like orbitals are the dominant fragment orbitals used for the cluster formation. The HOMO, $24a_1$, and the orbital directly below it, $18b_1$, are the two unbridged Os–Os bonds and are composed of fragment e_g-like orbitals. A narrow energy gap separates these two orbitals from a manifold of closely spaced molecular orbitals. These orbitals are predominantly t_{2g}-like but contain some destabilized Cl_2 character. Another narrow energy gap separates the low-energy Cl_2 orbitals. These orbitals represent both Os–Cl–Os interactions and Cl lone pairs. The composition of the $(\mu\text{-Cl})_2Os_3(CO)_{10}$ molecular orbitals are listed in Table VI.

The formation of the cluster will be presented in terms of the t_{2g}- and e_g-like fragment orbitals. In the neutral $Os(CO)_3$ and $Os(CO)_4$ fragments, the orbital populations are $(10a')^{2.0}(11a')^{2.0}(7a')^{2.0}(12a')^{2.0}(8a'')^{0.0}(13a')^{0.0}$ and $(6b_2)^{2.0}$-$(3a_2)^{2.0}(9a_1)^{2.0}(6b_1)^{2.0}(10a_1)^{0.0}$, respectively. The final cluster populations for $Os(CO)_3$ and $Os(CO)_4$ are $(10a')^{2.0}(11a')^{2.0}$-$(7a'')^{2.0}(12a')^{0.9}(8a'')^{0.3}(13a')^{0.3}$ and $(6b_2)^{2.0}(3a_2)^{2.0}(9a_1)^{2.0}$-$(6b_1)^{1.1}(10a_1)^{0.9}$, respectively. Accounting for the net loss of electron population in the two $Os(CO)_3$ fragments, the Cl_2 moiety's $5\sigma_u$ gains electron density. The elongated Cl_2 molecule has a population of $(5\sigma_g)^{2.0}(2\pi_u)^{4.0}(2\pi_g)^{4.0}(5\sigma_u)^{0.0}$ before cluster formation and a population of $(5\sigma_g)^{1.8}(2\pi_u)^{3.6}$-$(2\pi_g)^{3.5}(5\sigma_u)^{1.7}$ after cluster formation. The increased population of $5\sigma_u$ breaks the Cl–Cl bond.

Molecular Orbital Plots. In order to better understand the bonding in the $(\mu\text{-H})(\mu\text{-Cl})Os_3(CO)_{10}$ and $(\mu\text{-Cl})_2Os_3(CO)_{10}$ clusters, orbital plots have been made of the important Os–Os and Os–Y (Y = H, Cl) bonding orbitals. The orbital plots are very useful in elucidating the cluster bonding because individual bonds may be delocalized over several MO's. Two planes have been selected in order to delineate the atomic interactions within a single orbital. One of the planes contains the two osmium atoms and the bridging chlorine or hydrogen atom. This plane will be referred to as the wedge plane. The second plane bisects the two bridged osmium atoms and is perpendicular to the triosmium plane. This plane contains both the bridging atoms and the Os atom from the "back" $Os(CO)_4$ fragment. The triangle, Δ, represents the center of the intramolecular axis joining the two bridged Os atoms. This plane will be designated as the diagonal plane.

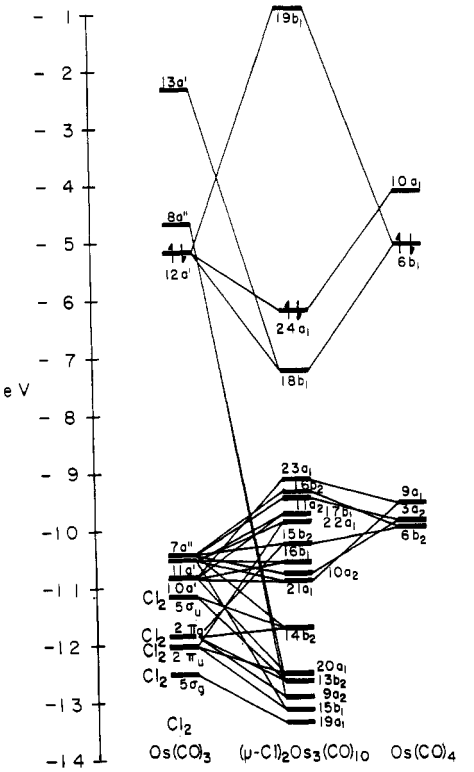

Figure 4. Molecular orbital bonding scheme for $(\mu\text{-Cl})_2Os_3(CO)_{10}$. The energy values were obtained from a Fenske–Hall calculation. Connectivity lines indicate the principal contributions to each molecular orbital.

$(\mu\text{-H})(\mu\text{-Cl})Os_3(CO)_{10}$. The wedge planes for the more important orbitals with large Cl character are shown in Figure 5. Molecular orbitals 25a″, 28a′, and 29a′ contain most of the Cl–Os bonding interactions. The 29a″ orbital has substantial Cl character, but the Os–Cl interaction is weakly antibonding. This orbital overlaps and affects the shape of the t_{2g}*-like manifold. The diagonal planes in Figure 6 show that 28a′ is mainly in the Os–Cl–Os plane, while 29a′ is nearly perpendicular to that plane.

The Os–H bonding interactions are shown in the wedge plane (Figure 7) and the diagonal plane (Figure 6). The Os–H–Os bonding interaction is split into two molecular orbitals due to the admixture of Cl 3p. By counting the number of contours along the Os–Os and Os–H internuclear axis, one

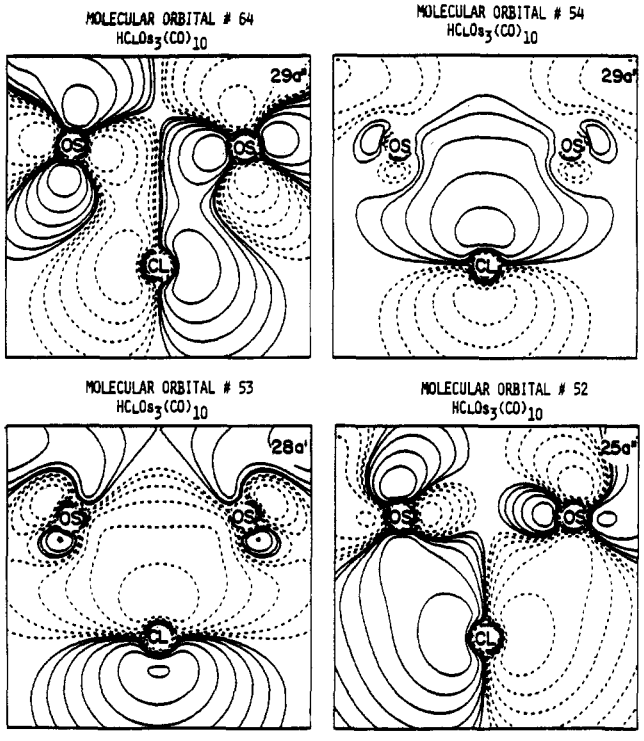

Figure 5. Orbital plots of 29a″, 29a′, 28a′, and 25a″ in the Os–Cl–Os wedge plane of $(\mu\text{-H})(\mu\text{-Cl})Os_3(CO)_{10}$. The lowest contour values are 2.44×10^{-4} e au^{-3}, and each succeeding contour differs from the previous one by a factor of 2.0.

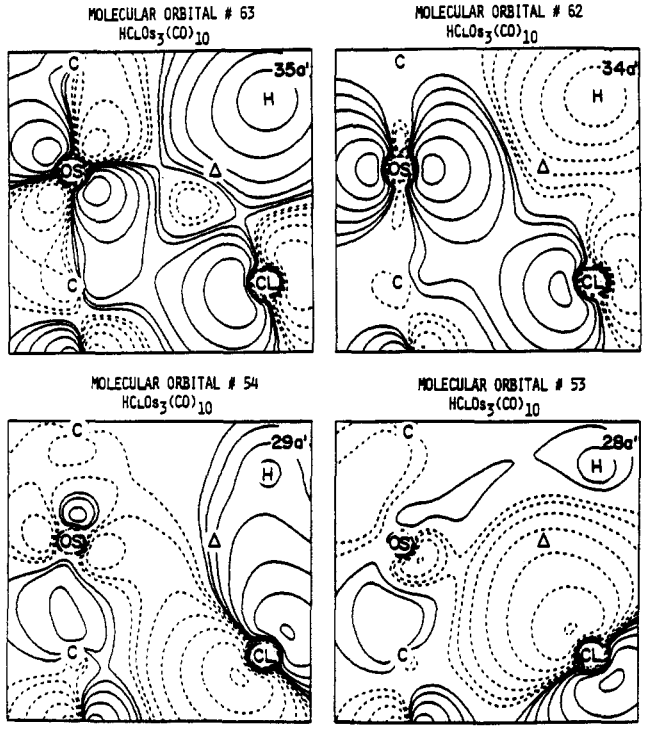

Figure 6. Orbital plots of 35a′, 34a′, 29a′, and 28a′ in the diagonal plane of $(\mu\text{-H})(\mu\text{-Cl})Os_3(CO)_{10}$. See text for complete definition of plane. The lowest contour values are 2.44×10^{-4} e au^{-3}, and each succeeding contour differs from the previous one by a factor of 2.0.

determines that the 34a′ and 35a′ show weak Os–Os and strong Os–H bonding interactions. The Os–H antibonding orbitals occur at much higher orbital energies and are unoccupied. The 35a′ in Figure 6 clearly shows both the Os–H–Os interaction and the mixing with Cl 3p, which destabilizes this orbital.

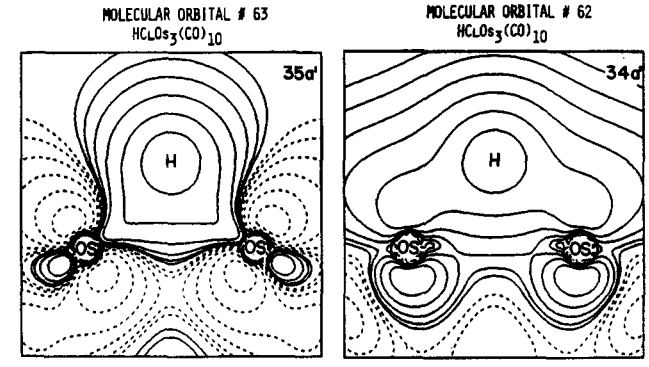

Figure 7. Orbital plots of 35a′ and 34a′ in the Os–H–Os wedge plane of $(\mu\text{-H})(\mu\text{-Cl})Os_3(CO)_{10}$. The lowest contour values are 2.44×10^{-4} e au^{-3}, and each succeeding contour differs from the previous one by a factor of 2.0.

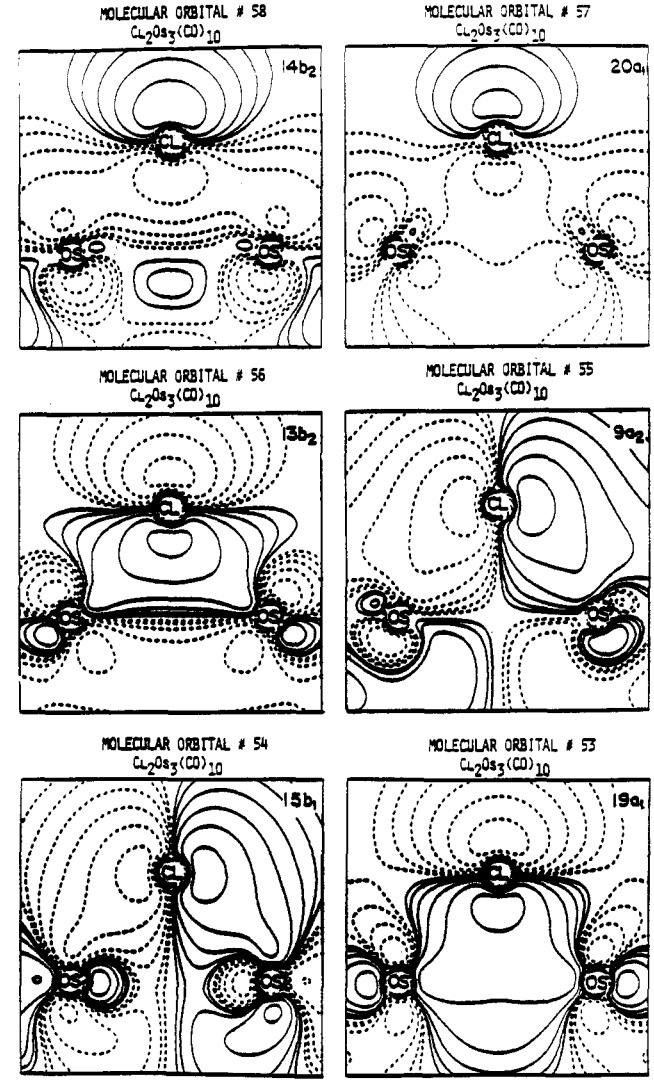

Figure 8. Orbital plots of $14b_2$, $20a_1$, $13b_2$, $9a_2$, $15b_1$, and $19a_1$ in the Os–Cl–Os wedge plane of $(\mu\text{-Cl})_2Os_3(CO)_{10}$. The lowest contour values are 2.44×10^{-4} e au^{-3}, and each succeeding contour differs from the previous one by a factor of 2.0.

$(\mu\text{-Cl})_2Os_3(CO)_{10}$. Two planes, the wedge with only one Cl atom (Figure 8) and the diagonal (Figure 9), will be used to present the Os–Cl interactions. The plots suggest that $19a_1$ is both Cl–Cl bonding and Os–Cl bonding. The $15b_1$ and $9a_2$ orbitals are Cl $3p_x$ symmetric and antisymmetric combinations, respectively. Both of these orbitals are Cl–Os bonding. The $13b_2$ and $20a_1$ orbitals are the Cl $3p_y$ antisymmetric and

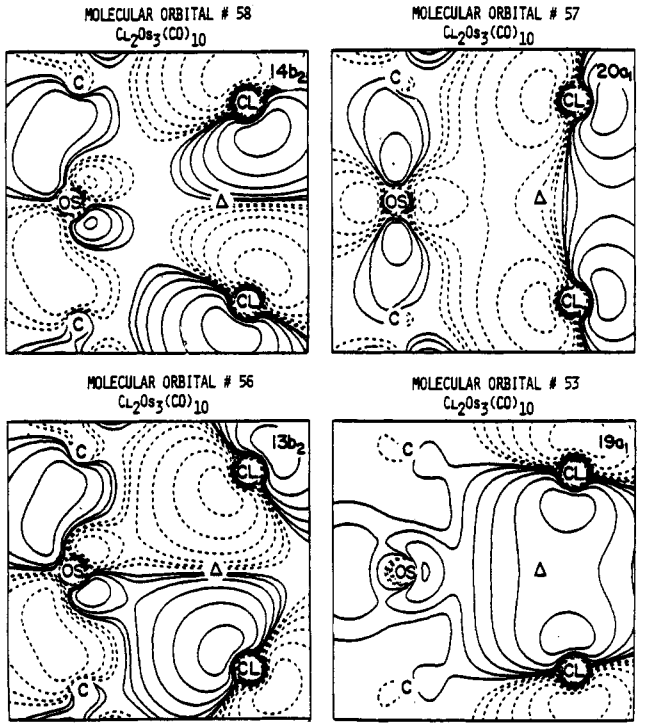

Figure 9. Orbital plots of $14b_2$, $20a_1$, $13b_2$, and $19a_1$ in the diagonal plane of $(\mu\text{-Cl})_2Os_3(CO)_{10}$. See text for complete definition of plane. The lowest contour vaues are 2.44×10^{-4} e au^{-3}, and each succeeding contour differs from the previous one by a factor of 2.0.

symmetric combinations, respectively. These two MO's are only weakly Cl–Os bonding and may be considered essentially nonbonding. The $14b_2$ MO is characterized by an antibonding Cl $3p_z$ interaction and contains little bonding with Os.

Discussion

Photoelectron Spectra. The calculated one-electron orbitals obtained from the Fenske–Hall calculations correlate reasonably well with the observed ionization energies in the PE spectra.[24,31] To simplify the description of the PE spectra, it can be divided into three regions. The first region spans from 7.5 to 8.5 eV, the second region covers 8.5 to 10.7 eV, and the third region extends from 10.7 to 13.5 eV. The interested reader may wish to review the PE spectra and peak assignments for both $Os_3(CO)_{12}$ and $(\mu\text{-H})_2Os_3(CO)_{10}$;[24] our assignments build on this previous work.

$(\mu\text{-H})(\mu\text{-X})Os_3(CO)_{10}$ (X = Cl, Br, I). The first two peaks in the first region correspond to the cluster's 36a′ and 30a″ MO's. These MO's are essentially the symmetric and antisymmetric combinations of the two Os–Os bonds formed between each $Os(CO)_3$ and $Os(CO)_4$ fragment. When compared to the PE spectrum of $Os_3(CO)_{12}$, the metal–metal IE region of these bridged triosmium systems appears to have lost intensity. This is consistent with three direct Os–Os bonds in $Os_3(CO)_{12}$ but only two direct Os–Os bonds in all $(\mu\text{-X})(\mu\text{-Y})Os_3(CO)_{10}$.

The second region contains two broad, overlapping ionization bands, which represent the t_{2g}*- and t_{2g}-like ionizations. These t_{2g}-like orbitals are well separated from the e_g-like orbitals, as predicted by our calculations. The leading edge of the t_{2g}*-like band (29a″, 35a′) contains some Cl 3p due to Os–Cl antibonding interactions. Our calculations show the IE for the leading edge decreases (9.1, 8.8, 8.5 eV) and the percent halogen character increases (24, 48, 85%) as one proceeds from Cl to Br to I. The IE trend correlates with the halogen's electronegativity. The remaining t_{2g}-like orbital energies are closely spaced; hence, no attempt will be made to assign the individual IE peaks. The small peak occurring on the high-energy side of the t_{2g} manifold is the t_{2g}-like combination with the d-orbital lobes pointed along the bridged Os–Os internuclear axis (30a′). As one proceeds from Cl to Br to I, this t_{2g}-like bonding interaction shifts to less stable IE's (10.4, 10.3, 10.1 eV). Changes in halogen character also affect the intensity in the t_{2g} region.

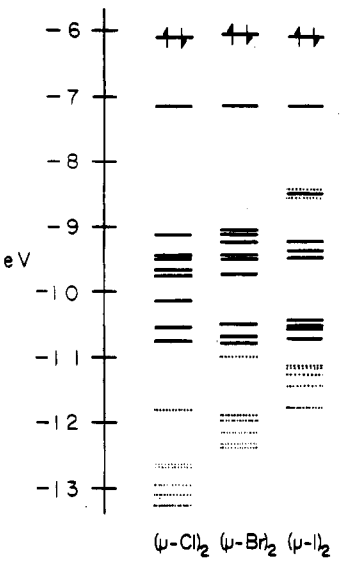

Figure 10. Molecular orbital values for $(\mu\text{-X})_2Os_3(CO)_{10}$ (X = Cl, Br, I), which were obtained from a Fenske–Hall calculation. The molecular orbitals with more than 40% halogen character are shown as dotted lines.

There are several ionizations occurring in the third region. The first and most intense band (25a″, 28a′, 29a′) corresponds to overlapping Os–X interactions and the nonbonding halogen p orbitals (lone pairs). This band shifts toward lower IE's as the halogens change from Cl to Br to I. This band is separated into two individual bands for the I derivative, due, in part, to I spin–orbit coupling. The intensities of these bands also decrease, suggesting that the halogen character is decreasing and the Os character is increasing. Trailing the Os–halogen bands are the Os–H–Os interactions, which span 12.2–13.2 eV. This range correlates well with the published results of 11.0–13.5 eV for bridging hydrogens in transition-metal clusters.[24b,c,32] The Os–H–Os interaction mixes with both the halogen 3p and the t_{2g}-like orbitals on Os. This Os–H–Os ionization becomes less stable as one proceeds from Cl to Br to I.

$(\mu\text{-X})_2Os_3(CO)_{10}$ (X = Cl, Br, I). The two IE peaks in the first region correspond to the two $Os(CO)_3$–$Os(CO)_4$ Os–Os bonds ($24a_1$, $18b_1$). The first band for the Br compound shifts slightly to higher IE, when compared to that of the Cl derivative. The two peaks in the Cl derivative have the same intensity, while the intensity of the first peak decreases and the second increases for Br. The I derivative's corresponding first peak is not observed, while the second peak is very intense. Our calculations suggest that these peaks merge because of increased I character. Our calculated MO energies, showing

(31) (a) Lichtenberger, D. L.; Fenske, R. F. *Inorg. Chem.* **1976**, *15*, 2015. (b) Lichtenberger, D. L.; Fenske, R. F. *J. Am. Chem. Soc.* **1976**, *98*, 50. (c) Block, T. F.; Fenske, R. F. *Ibid.* **1977**, *99*, 4321. (d) Hubbard, J. L.; Lichtenberger, D. L. *Inorg. Chem.* **1980**, *19*, 1388. (e) Morris-Sherwood, B. J.; Kolthammer, B. W. S.; Hall, M. B. *Ibid.* **1981**, *20*, 2771. (f) DeKock, R. L.; Wong, K. S.; Fehlner, T. P. *Ibid.* **1982**, *21*, 3203.

(32) (a) Green, J. C.; Seddon, E. A.; Mingos, D. M. P. *J. Chem. Soc., Chem. Commun.* **1979**, 94. (b) Green, J. C.; Mingos, D. M. P.; Seddon, E. A. *J. Organomet. Chem.* **1980**, *185*, C20. (c) Wong, K. S.; Dutta, T. K.; Fehlner, T. P. *Ibid.* **1981**, *215*, C48. (d) Green, J. C.; Mingos, D. M. P.; Seddon, E. A. *Inorg. Chem.* **1981**, *20*, 2595. (e) Chesky, P. T.; Hall, M. B. *Inorg. Chem.* **1983**, *22*, 2998 (part four).

Table VII. Mulliken Overlap Populations for $XYOs_3(CO)_{10}$ (X = Cl; Y = Cl, H)

		osmium-XY			osmium-osmium				
XY	bond[a]	t_{2g}	e_g	$13a_1$	total	d-d	e_g-e_g	t_{2g}-t_{2g}	13a′-13a′
HCl	Os-Os*				0.2275	0.0175	0.1681	−0.0052	
	Os-Os	−0.0169	0.1992	0.0842	0.0511	0.0050	0.0025	−0.0021	0.0256
Cl_2	Os-Os*				0.2275	0.0211	0.1670	−0.0092	
	Os-Os	−0.0278	0.1944	0.1010	−0.0264	−0.0033	0.0023	−0.0006	−0.0115

[a] Os represents one of the two Os's in the $Os(CO)_3$ fragments. Os* represents the Os in the $Os(CO)_4$ fragment.

the shifting halogen character, are shown in Figure 10. Our predicted IE for the first two e_g-like orbitals is too low. If one collapses the energy gap between the two highest occupied MO's and shifts their molecular orbitals to higher IE's so that they resemble the experimental values, it becomes clear how the change from Cl to Br to I affects the first band in the PE spectra. The low-energy MO's of increased I character now merge with the two bonding $(CO)_3Os$–$Os(CO)_4$ orbitals, creating only one intense band.

The second region contains overlapping ionization bands, which represent the t_{2g}*- and t_{2g}-like ionizations. The leading edge of the t_{2g}*-like ionizations ($23a_1$, $16b_2$) contains Cl 3p. As one proceeds from Cl to Br to I, the leading edges of the t_{2g}*-like bands move to lower IE's. The more stable, albeit less intense, bands above 9.7 eV correspond to the t_{2g}-like ionizations. The increased intensity of the trailing edge, while one proceeds from Cl to Br to I, suggests that the t_{2g}-like orbitals are interacting with bridging ligands. In the case of I, the increase in intensity reflects the increasing halogen contribution. The other t_{2g}-like orbital energies are closely spaced; hence, no attempt will be made to assign the individual IE peaks.

The third region is characterized by the X–Os bonding and nonbonding halogen (lone pair) interactions. The ionization band shifts toward lower IE's and separates into distinctive peaks as one proceeds from Cl to Br to I. The MO's $13b_2$ and $20a_1$ correspond to the nonbonding Cl p orbital (lone pair) asymmetric and symmetric combinations, respectively. At more stable IE's, the $19a_1$ and $15b_1$ represent the bonding Cl p orbitals (Os–Cl interactions). The corresponding asymmetric combination of $19a_1$, $14b_2$, is the small peak that occurs between the second the third ionization regions. In Br this peak, which is still distinguishable, shifts to the high-energy side of the t_{2g}-like manifold. In I this band shifts to lower IE and mixes with the t_{2g}-like orbitals, as shown in Figure 10. As one proceeds from Cl to Br to I, the IE band broadens due to the halogen symmetric and asymmetric combinations moving to lower IE's along with the halogen lone pairs. Spin–orbit coupling effects on I help to create the individual IE peaks.

Nature of the Bonding. Fenske–Hall molecular orbital calculations and PE spectra of $Os_3(CO)_{12}$ and $(\mu\text{-H})_2Os_3(CO)_{10}$ have been reported.[24b] The molecular orbital results suggested that the t_{2g}-like electrons undergo rearrangement, forming a partial Os–Os bond between the hydrogen-bridged osmium atoms. The calculations also suggested that electron donation into a low-lying, unoccupied antibonding Os–Os orbital is the reason for the increase in the bridged osmiums' bond distance when H atoms are replaced by atoms that are both "σ" and "π" electron donors. Figure 11 shows the calculated eigenvalues (MO energies) for $(\mu\text{-H})_2Os_3(CO)_{10}$, $(\mu\text{-H})(\mu\text{-Cl})Os_3(CO)_{10}$, and $(\mu\text{-Cl})_2Os_3(CO)_{10}$. Comparing H_2 to HCl to Cl_2 bridges, we see HOMO and LUMO energy levels decrease and increase, respectively. The decreasing HOMO energy level and increasing LUMO–HOMO energy gap both signify enhanced stability of the cluster. The rectangles for all three clusters represent the t_{2g}-like orbitals. The substitution of a Cl for a H shows how the Cl interacts with the Os–H–Os bond by sending substantial Os–H–Os character to higher IE (shown inside the rectangle). The addition of

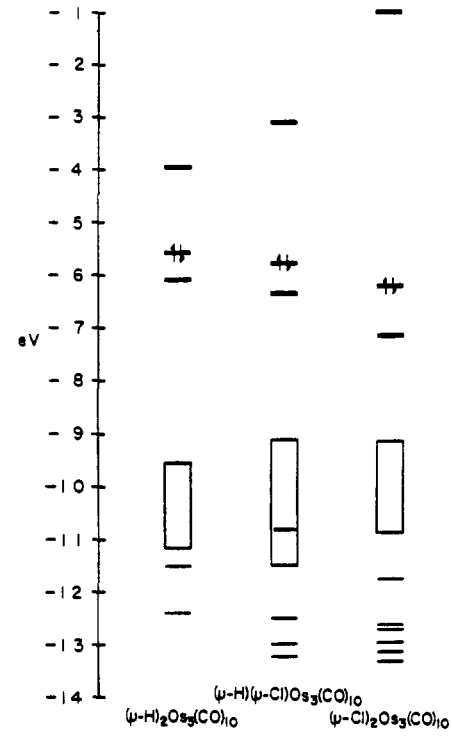

Figure 11. Molecular orbital energies for $(\mu\text{-H})_2Os_3(CO)_{10}$, $(\mu\text{-H})(\mu\text{-Cl})Os_3(CO)_{10}$, and $(\mu\text{-Cl})_2Os_3(CO)_{10}$, which were obtained from a Fenske–Hall calculation. The rectangle designates the t_{2g}-like orbitals in each cluster. The orbitals with more than 50% character in the bridging atoms (H and Cl) are shown as horizontal lines.

the second Cl atom leads to a mixing of Cl–Os bonding and Cl lone-pair interactions.

The Fenske–Hall calculations can be used to describe additional details of the electronic structure and bonding in the triosmium decacarbonyl clusters. Through the use of overlap populations, one observes little mixing between the t_{2g}- and e_g-like orbitals. This is due to both the large energy separation ($10Dq$) between the O_h e_g and t_{2g} orbitals for a third-row transition-metal atom and the relative geometry enforced by the carbonyls in the osmium carbonyl fragments.[29] Additional features will be discussed for each triosmium cluster below.

$(\mu\text{-H})(\mu\text{-Cl})Os_3(CO)_{10}$. The calculated overlap populations for the Os–Os interactions are shown in Table VII. The total Os–Os overlap population is greater for the Os–Os* (Os* represents the Os in $Os(CO)_4$) bond than for the bond between the two bridged $Os(CO)_3$ fragments. The Os–Os* bond consists primarily of Os e_g–e_g orbital interactions. The Os–Os total overlap population suggests that the formal bond order is nearly zero. The $Os(CO)_3$ fragments' diffuse 13a′ orbital has some positive overlap population and may contribute to a small net Os–Os bonding interaction.

The overlap populations for HX (X = Cl, Br, I) moieties when bonded to triosmium decacarbonyl were zero. As expected, H–X may be considered as two separate atoms bound to the two $Os(CO)_3$ fragments. The donation of electron density from the Os atoms to the antibonding LUMO of H–X destroys the H–X bonding character. The primary Os–HX

Table VIII. Gross Mulliken Atomic Charges in $XYOs_3(CO)_{10}$ Clusters

XY	gross atomic charges			
	Os[a]	Os*[b]	X	H
HCl	0.303+	0.191-	0.345-	0.422-
HBr	0.287+	0.192-	0.296-	0.424-
HI	0.276+	0.194-	0.252-	0.427-
Cl_2	0.233+	0.237-	0.328-	
Br_2	0.210+	0.243-	0.328-	
I_2	0.190+	0.248-	0.252-	

[a] Os represents one of the two Os's in the $Os(CO)_3$ fragments. [b] Os* represents the Os in the $Os(CO)_4$ fragment.

interaction is through the e_g-like and 13a' orbitals. Table VIII shows the Mulliken atomic charges, which show a definite shift of electron density from the two bridged Os atoms to Os* and the bridging atoms.

$(\mu$-Cl)$_2$Os$_3$(CO)$_{10}$. The overlap populations in Table VII indicate that the Os–Os* bond is equivalent in strength to the Os–Os* bond in the HX derivatives. The Os–Os overlap population suggests no direct M–M bonding between the two $Os(CO)_3$ fragments. The $Os(CO)_3$ fragments' diffuse 13a' orbitals have a negative overlap population, and this may contribute to an overall Os–Os antibonding interaction. As expected, the overlap populations for X_2 (X = Cl, Br, I) when bonded to the triosmium decacarbonyl moiety were found to be essentially zero. The donation of Os electron density to the antibonding LUMO of X_2 eliminates the bonding in the X_2 molecule.

The Mulliken atomic charges, shown in Table VIII, indicate the shift of electron density from the $Os(CO)_3$ fragments to the bridging halogens. The Os* atoms become more negative as the halogens change from Cl to Br to I. Our calculations suggest that the halogens interact with the Os* indirectly through the bridging Os. This interaction was also hinted by the destabilization of the t_{2g}-like peaks in the PE spectra.

Conclusion

The PE spectra and MO calculations suggest that the only direct Os–Os bonds in both of these bridging series are the two $(CO)_4Os$–$Os(CO)_3$ bonds. The $(CO)_3Os$–$Os(CO)_3$ interaction in the $(\mu$-H)$(\mu$-X) series is weakly bonding due to the diffuse 13a' interactions, while that in the $(\mu$-X$)_2$ series is weakly antibonding. The MO calculations suggest that the t_{2g}-like $Os(CO)_3$ orbitals, which are usually considered only M–CO π bonding, interact strongly with the bridging H and halogen atoms. Changes in the PE spectra are observed as a result of this interaction.

Acknowledgment is made to the Robert A. Welch Foundation (Grant A-648) and the National Science Foundation (Grant CHE 79-20993) for support of this work.

Registry No. 1, 12557-93-6; (μ-H)(μ-Br)$Os_3(CO)$, 61199-98-2; (μ-H)(μ-I)$Os_3(CO)_{10}$, 61199-99-3; (μ-Cl)$_2Os_3(CO)_{10}$, 28109-18-4; (μ-Br)$_2Os_3(CO)_{10}$, 28109-19-5; (μ-I)$_2Os_3(CO)_{10}$, 87101-94-8.

Contribution from the Istituto FRAE-CNR, Bologna, Italy, Istituto Chimico "G. Ciamician", University of Bologna, Bologna, Italy, and Institute of Inorganic Chemistry, University of Fribourg, Fribourg, Switzerland

Excited-State Properties of Complexes of the Ru(diimine)$_3^{2+}$ Family

FRANCESCO BARIGELLETTI,[1] ALBERTO JURIS,[1,2] VINCENZO BALZANI,*[1,2] PETER BELSER,[3] and ALEX VON ZELEWSKY*[3]

Received February 15, 1983

The absorption spectra, emission spectra, emission lifetimes, and temperature dependence of emission intensity and lifetime (between 84 and 330 K) of the complexes $Ru(bpy)_3^{2+}$, $Ru(bpy)_2(biq)^{2+}$, and $Ru(biq)_3^{2+}$ are reported (bpy = 2,2'-bipyridine, biq = 2,2'-biquinoline). The $Ru(biq)_3^{2+}$ complex exhibits metal-to-ligand charge-transfer absorption and emission bands red shifted by about 3000 cm^{-1} compared with the corresponding bands of $Ru(bpy)_3^{2+}$. In the mixed-ligand complex, distinct Ru → bpy and Ru → biq charge-transfer absorptions are present, but emission only occurs from the lowest excited state, which is a Ru → biq charge-transfer state. The temperature dependence of the luminescence emission indicates that in $Ru(biq)_3^{2+}$ a short-lived excited state (most likely a triplet metal-centered state) lies 2700 cm^{-1} above the emitting charge-transfer level. In $Ru(bpy)_2(biq)^{2+}$, there are two low-lying Ru → biq charge-transfer excited states separated by 400 cm^{-1} which presumably originate from the splitting of the metal t_{2g} orbitals in the reduced C_{2v} symmetry of the complex, while the lowest triplet metal-centered excited state lies more than 5500 cm^{-1} above. The photochemical implications of these results are briefly discussed.

Introduction

Complexes of the Ru(diimine)$_3^{2+}$ family, particularly Ru(bpy)$_3^{2+}$, have recently been the object of much interest because of their unique excited-state properties[4-7] and of their use as photosensitizers in the photochemical conversion of solar energy.[7-12] There has also been some controversy concerning the exact nature of the emitting excited state and of the other excited states which are of importance for the photochemical and photophysical properties.[4,6,13-17] In an attempt to understand the details of the electronic states of such complexes and with the aim of tuning their properties in a controlled manner, we have synthesized[18] a series of Ru(II) complexes with ligands of different size and different electronic structure

(1) Istituto FRAE-CNR.
(2) University of Bologna.
(3) University of Fribourg.
(4) Crosby, G. A. *Acc. Chem. Res.* **1975**, *8*, 231.
(5) Kemp, T. J. *Prog. React. Kinet.* **1980**, *10*, 301.
(6) DeArmond, M. K.; Carlin, C. M. *Coord. Chem. Rev.* **1981**, *36*, 325.
(7) Kalyanasundaram, K. *Coord. Chem. Rev.* **1982**, *46*, 159.
(8) Meyer, T. J. *Isr. J. Chem.* **1977**, *15*, 200.
(9) Balzani, V.; Bolletta, F.; Gandolfi, M. T.; Maestri, M. *Top. Curr. Chem.* **1978**, *75*, 1.
(10) Sutin, N.; Creutz, C. *Pure Appl. Chem.* **1980**, *52*, 2717.
(11) Whitten, D. G. *Acc. Chem. Res.* **1980**, *13*, 83.
(12) Graetzel, M. *Acc. Chem. Res.* **1981**, *14*, 376.
(13) Hager, G. D.; Crosby, G. A. *J. Am. Chem. Soc.* **1975**, *97*, 7031. Hager, G. D.; Watts, R. J.; Crosby, G. A. *Ibid.* **1975**, *97*, 7037.
(14) Felix, F.; Ferguson, J.; Güdel, H. U.; Ludi, A. *Chem. Phys. Lett.* **1979**, *62*, 153. Felix, F.; Ferguson, J.; Güdel, H. U.; Ludi, A. *J. Am. Chem. Soc.* **1980**, *102*, 4096. Ferguson, J.; Herren, F. *Chem. Phys. Lett.* **1982**, *89*, 371. Ferguson, J.; Krausz, E. R. *Ibid.* **1982**, *93*, 21.
(15) Vanquickenborne, L. G.; Ceulemans, A. *Inorg. Chem.* **1978**, *17*, 2730. Ceulemans, A.; Vanquickenborne, L. G. *J. Am. Chem. Soc.* **1981**, *103*, 2238.
(16) Belser, P.; Daul, C.; von Zelewsky, A. *Chem. Phys. Lett.* **1981**, *79*, 596.
(17) Kober, E. M.; Meyer, T. J. *Inorg. Chem.* **1982**, *21*, 3967.
(18) Belser, P.; von Zelewsky, A. *Helv. Chim. Acta* **1980**, *63*, 1675.

0020-1669/83/1322-3335$01.50/0